ELSEVIER

Chemical Geology 212 (2004) 269–277

CHEMICAL GEOLOGY
INCLUDING
ISOTOPE GEOSCIENCE

www.elsevier.com/locate/chemgeo

# Hydrothermal phase stabilization of 2-line ferrihydrite by bacteria

C.B. Kennedy[1], S.D. Scott, F.G. Ferris*

*Department of Geology, University of Toronto, 22 Russell Street, Toronto, Ontario, Canada M5S 3B1*

Received 28 January 2004; accepted 16 August 2004

**Abstract**

Poorly ordered 2-line ferrihydrite deposits from the caldera of Axial Volcano, a site of hydrothermal vent activity along the Juan de Fuca Ridge, are characterized by an abundance of bacterial structures resembling *Gallionella ferruginea*, *Leptothrix ochracea* and PV-1 filaments encrusted with nanoparticulate ferrihydrite. Ferrihydrite formed in the absence of bacteria can be metastable and will subsequently react to form more structurally ordered iron oxide phases such as hematite or goethite. Inspection of samples from 2-day 80 °C aqueous heating experiments by electron microscopy and X-ray diffraction revealed that a natural sample of bacteriogenic ferrihydrite from Axial Volcano did not undergo a phase transition, whereas synthetic ferrihydrite, absent of bacteria, transformed to hematite after 2 days. A series of bacterial-ferrihydrite composites exhibited decreasing amounts of transformation to hematite with increased amounts of Fe(III) bound to bacteria. Complete inhibition was observed when 50% of the total Fe was bound as ferric iron and 50% was present as ferrihydrite. For the synthetic ferrihydrite samples containing bacteria, the inhibition of ferrihydrite transformation is attributed to microbial surface functional groups (i.e. carboxyl, phosphoryl, amine) constraining the Brownian motion of surface bound ferrihydrite nanoparticles, thereby eliminating the aggregation and rotation of particles required for crystal growth. The stabilization of ferrihydrite will prolong the longevity of a highly reactive mineral phase, which may have implications for marine geochemistry and environmental remediation. Preservation of bacteria encrusted with transformation resistant ferrihydrite may enhance the potential usefulness of bacteriogenic ferrihydrite to harbour bacterial microfossils, imparting these types of samples with potential use for paleontology and astrobiology.


*Keywords:* Bacteria; Ferrihydrite; Phase transition; Inhibition; Hydrothermal; Axial Volcano

## 1. Introduction

The poorly ordered iron oxyhydroxide mineral 2-line ferrihydrite (termed simply herein as ferrihydrite) is commonly found on the sea floor in the proximity of low temperature (i.e. <25 °C) hydrothermal vents along mid-ocean ridges (MORs) and on seamounts (Alt, 1988; Binns et al., 1993; Boyd et al., 1993). This mineral is commonly intermixed with lithoautotrophic

* Corresponding author. Tel.: +1 416 978 0526; fax: +1 416 978 3938.

*E-mail address:* ferris@geology.utoronto.ca (F.G. Ferris).

[1] Present address: Deep Biosphere Laboratory, CMB-Microbiology, Göteborg University, Box 462, SE-405 30, Göteborg, Sweden.

0009-2541/$ - see front matter © 2004 Elsevier B.V. All rights reserved.
doi:10.1016/j.chemgeo.2004.08.017

Fe(II) oxidizing bacteria, which have been implicated as causative agents in the formation of ferrihydrite (Alt, 1988; Juniper and Fouquet, 1988; Juniper and Sarrazin, 1995; Juniper and Tebo, 1995; Fortin et al., 1998; Emerson and Moyer, 2002; Kennedy et al., 2003a). The bacteria also behave as geochemically reactive solids (Fortin et al., 1997), capable of adsorbing Fe and subsequently acting as a site for heterogeneous surface nucleation (Warren and Ferris, 1998; Smith and Ferris, 2003). Ferrihydrite formed in the absence of bacteria can rapidly (on the order of days) transform to more structurally ordered iron oxide phases such as hematite or goethite (Cornell and Schwertmann, 1996), resulting in a decrease in surface reactivity of the mineral and alteration of its morphological characteristics.

Previous studies have established that the phase transition of ferrihydrite is dependent on inorganic factors such as pH and the presence of adsorbed cations and anions (Schwertmann and Murad, 1983; Zhao et al., 1994; Kukkadapu et al., 2003). While the abiotic factors of ferrihydrite's phase transition have been well characterised, the effect of bacteria in this process has not been investigated. From the apparent lack of structurally ordered iron oxides intermixed with bacteria in marine environments (Kennedy et al., 2003a), and the study by Banfield et al. (2000) documenting less extensive coarsening of ferrihydrite bound to microbial surfaces, this investigation was performed to determine whether bacteria could inhibit the phase transition of ferrihydrite under hydrothermal conditions.

## 2. Materials and methods

### 2.1. Sample collection

Natural samples were collected at both active and inactive low temperature (~10 °C) hydrothermal vent sites throughout the caldera of Axial Volcano during the New Millenium Observatory (NeMO) expedition in July 2000 and June 2001 aboard NOAA's vessel Ronald H. Brown. Axial Volcano is situated on the Juan de Fuca Ridge in the north-east Pacific Ocean with its caldera at a depth of approximately 1500 m (Johnson and Embley, 1990). The iron oxide deposits sampled included mound-like (~0.1–0.5 m high) accretions to widespread blanket-type deposits. Samples were collected using a suction sampler attached to the Canadian ROPOS remotely operated vehicle (ROV).

### 2.2. Synthetic ferrihydrite preparation

The precipitation of synthetic ferrihydrite was accomplished by the gradual titration of $Fe(NO_3)_3 \cdot 9H_2O$ (0.4 mmol Fe) with 1 M NaOH to pH~7. The precipitate was centrifuged for 5 min at $3200 \times g$ and rinsed with 18 MΩ ultrapure water (UPW), with this cycle being repeated three times.

### 2.3. Growth conditions for Bacillus subtilis

Pure cultures of *B. subtilis* 168 were grown to exponential phase at 30 °C in Trypticase soy broth (Difco). Harvesting of the bacteria was accomplished by centrifugation for 10 min at $7000 \times g$ and rinsing with UPW, with this cycle being repeated three times. The bacteria were re-suspended in sterile UPW after washing.

### 2.4. Bacteria-synthetic ferrihydrite composites

Bacteria-synthetic ferrihydrite composites were prepared by combining specific concentrations of bacteria (see Table 1) in UPW (as determined from standard curves of dry weight at an optical density of 600 nm) with approximately 1 g of $Fe(NO_3)_3 \cdot 9H_2O$ (0.4 mmol Fe) solution at pH 2.5. The combined solutions were gently stirred for 1 h in order to

Table 1
Quantities of bacteria and Fe in the samples from the hydrothermal experiments

| Sample | mg bacteria/mmol Fe | b.c. mol/l[a] | M Fe | % bound[b] |
|---|---|---|---|---|
| A1 | 84.88 | 5.82E−04 | 3.16E−03 | 18 |
| A2 | 101.04 | 1.19E−03 | 4.36E−03 | 28 |
| A3 | 200.46 | 1.29E−03 | 3.51E−03 | 37 |
| A4 | 200.55 | 1.35E−03 | 3.38E−03 | 39 |
| A5 | 261.94 | 1.23E−03 | 2.80E−03 | 43 |
| A6 | 306.06 | 1.62E−03 | 2.99E−03 | 52 |
| A7 | 386.25 | 1.62E−03 | 2.58E−03 | 62 |

[a] The binding capacity (b.c.) was calculated from the value reported by Warren and Ferris (1998).

[b] Percent bound refers to the amount of ferric iron bound to *B. subtilus* as calculated using its binding capacity at the given molar concentration of Fe in MINEQL+(v.4.0).

promote sorption of Fe(III) to the bacterial surfaces and then slowly titrated to ~pH 7 with 1, 0.1 and 0.01 M NaOH. Finally, the samples were centrifuged for 5 min at 3000×*g* and rinsed with UPW, with this rinse cycle being repeated three times.

### 2.5. Hydrothermal experiments

Each of the three sample types were placed into 50-ml glass vials filled with UPW for a period of 2 days at 80 °C. This temperature and duration were selected because they are found to rapidly transform synthetic ferrihydrite in the absence of bacteria. At the end of each heating duration time, the samples were dried in an oven at 40 °C. A synthetic sample was also prepared as above, but not subjected to the elevated temperatures.

### 2.6. Scanning electron microscopy (SEM)

Approximately 1 ml of wet slurry from the samples before and after the hydrothermal experiments was fixed with 2% glutaraldehyde and filtered onto white nucleopore track-etch 0.2 μm membrane filters with 10 ml of 18 MΩ UPW. Filtered samples were dehydrated through a graded series of ethanol solutions (10%, 50%, 80% and 100% v/v). The filters remained in each ethanol solution for 7 min, left to stand in the 100% solution for 4 h and then placed in a dessicator overnight. Specimens were mounted on Al stubs and Au coated using a Cressington Sputter-Coater 108 at 0.06–0.08 mbar for 60 s. The samples were examined on a Hitachi S-2500 SEM with an accelerating voltage of 15 kV and a working distance of 21 mm.

### 2.7. Transmission electron microscopy (TEM)

Iron oxides from Axial Volcano were fixed with 2% glutaraldehyde and dehydrated in a series of ethanol solutions (25%, 50%, 75% and 100% v/v) for 15 min each. Infiltration by 50% (v/v) epoxy resin (TAAB) and ethanol proceeded for 1 h, then by the epoxy resin only for 1 h, followed by polymerization for 8–10 h at 60 °C. Ultra thin sections (0.2 μm) were cut with an Ultracut E ultramicrotome (Reichert-Jung), and collected on Formvar and carbon-coated copper grids (Marivac) and examined with a Phillips EM400 electron microscope.

### 2.8. X-ray diffraction (XRD)

Dried samples from each of the sample types were thoroughly crushed with a mortar and pestle. Approximately 0.2 g of powdered iron oxide was mixed with 1 ml of acetone in a plastic weighing dish and spread evenly over a glass slide. A Phillips XRD system with a PW1830 HT generator, PW 1050 goniometer and PW3710 electronics control was run at 40 kV and 40 mA with a lower pulse height distribution (PHD) of 44 and an upper PHD of 80 to aid in reduction of secondary iron fluorescence. The overall mineralogy of the samples was obtained by using Cu Kα radiation with a step size of 0.020 at a rate of 0.85 s/step from a $2\theta$ of 4° to 90°. For the bacterial-ferrihydrite composites a step size of 0.020 at a rate of 2.0 s/step from a $2\theta$ of 20° to 50° was used.

### 2.9. Data analysis

The phase transition inhibition of synthetic ferrihydrite was assessed by comparing XRD peak heights from the bacterial-synthetic ferrihydrite composites to a synthetic ferrihydrite sample after the 2-day heating exposure. Four peaks present in the XRD trace of hematite at an interplanar spacing of 3.6, 2.7, 2.5 and 2.2 Å were used for the comparison. Inhibition of ferrihydrite transformation was calculated by determining the relative percentage of peak height reduction compared to the non-bacterial standard.

The effect of bacterial quantity on ferrihydrite's phase transition was compared by determining the amount of ferric iron bound to bacteria and precipitated ferrihydrite at each of the given molar concentrations of Fe (Table 1). The geochemical modelling program MINEQL+ (v. 4.0) was used to determine the percentage of microbially bound ferric iron and calculated based on the $1\times10^{-3}$ mol $g^{-1}$ $cells^{-1}$ binding capacity of *B. subtilus* determined by Warren and Ferris (1998).

## 3. Results

The Axial Volcano sample was previously examined by XRD and revealed a diffraction trace that corresponded to 2-line ferrihydrite (Kennedy et al., 2003a). The sample is composed predominantly of

bacterial forms encrusted with nanoparticulate ferrihydrite that closely resemble *Leptothrix ochracea* sheaths (Emerson and Revsbech, 1994), *Gallionella ferruginea* stalks (Hallbeck and Pedersen, 1991) and PV-1 filaments (Emerson and Moyer, 2002) (Fig. 1). Inspection of all the samples by SEM after the hydrothermal experiments revealed that the ferrihydrite without bacteria formed micron sized aggregates, whereas no change was observed in the morphology of the bacterial ferrihydrite composite samples (Fig. 2).

There was no detectable structural change in the synthetic ferrihydrite sample that remained at room temperature for 2 days, as indicated by the lack of any peak development in its XRD trace. All samples prior to heating revealed two small broad reflections at 2.6 and 1.5 Å in their XRD trace. Fig. 3a illustrates the 2.6 Å reflection witnessed in all samples prior to heating. Ferrihydrite from Axial Volcano did not exhibit a change in its XRD trace after the hydrothermal transformation experiment. In contrast, the synthetic ferrihydrite sample (lacking bacteria) developed characteristic hematite peaks at 3.6, 2.7, 2.5 and 2.2 Å (Fig. 3), representing an increase in structural ordering of the iron oxide (Cornell and Schwertmann, 1996). Peak height in the XRD traces of the bacterial synthetic ferrihydrite composites decreased from the peak height witnessed in the non-bacterial sample to no detectable peak as the amount of bacteria in the composites increased (Fig. 3, Table 2).

The percentage of ferric iron bound to the microbial surfaces and corresponding peak inhibition for the 2.7 and 2.5 Å trace peaks is shown in Fig. 4. Extrapolation of these curves indicates that for *B. subtilus*, approximately 50% of the total Fe must be bound as ferric iron, while the remaining Fe is present as ferrihydrite in order for the ferrihydrite composites to remain stable under the hydrothermal conditions used for these experiments.

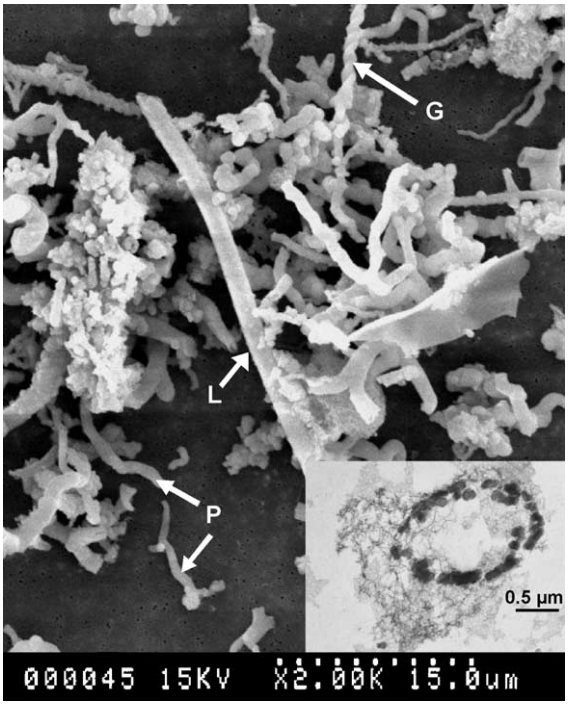


Fig. 1. SEM image of mineralized bacteria from the caldera of Axial Volcano resembling the sheath of *L. ochracea* (L), the stalk of *G. ferruginea* (G) and the non-helical filaments of PV-1 (P), as indicated. The inset TEM image is a cross-section of a bacterial structure encrusted with nanoparticulate ferrihydrite.

## 4. Discussion

The phase transition of ferrihydrite proceeds by the release of adsorbed water molecules to facilitate either particle aggregation and crystal growth, or dissolution and re-precipitation of more structurally ordered particles (Cornell and Schwertmann, 1996). This process has been advanced at the atomic scale in recent studies by Penn and Banfield (1999) and Banfield et al. (2000), who present a model of aggregation-based crystal growth for the phase transition of ferrihydrite. In their model, Brownian motion results in the aggregation and rotation of nanoparticles in an effort to attain the lowest possible free energy configuration in three dimensions. Crystal growth then proceeds by the desorption of water molecules at aggregated nanoparticle interfaces, allowing for the formation of iron–oxygen bonds. The elevated temperatures used in this study would have increased the rate of Brownian motion in the aqueous samples and the subsequent ability for the transformation of ferrihydrite to a more structurally ordered phase. In the case of the synthetic ferrihydrite sample lacking bacteria, Brownian motion would not have been inhibited, ultimately resulting in the coarsening and phase transition of ferrihydrite to hematite. In the synthetic ferrihydrite composites containing bacteria,

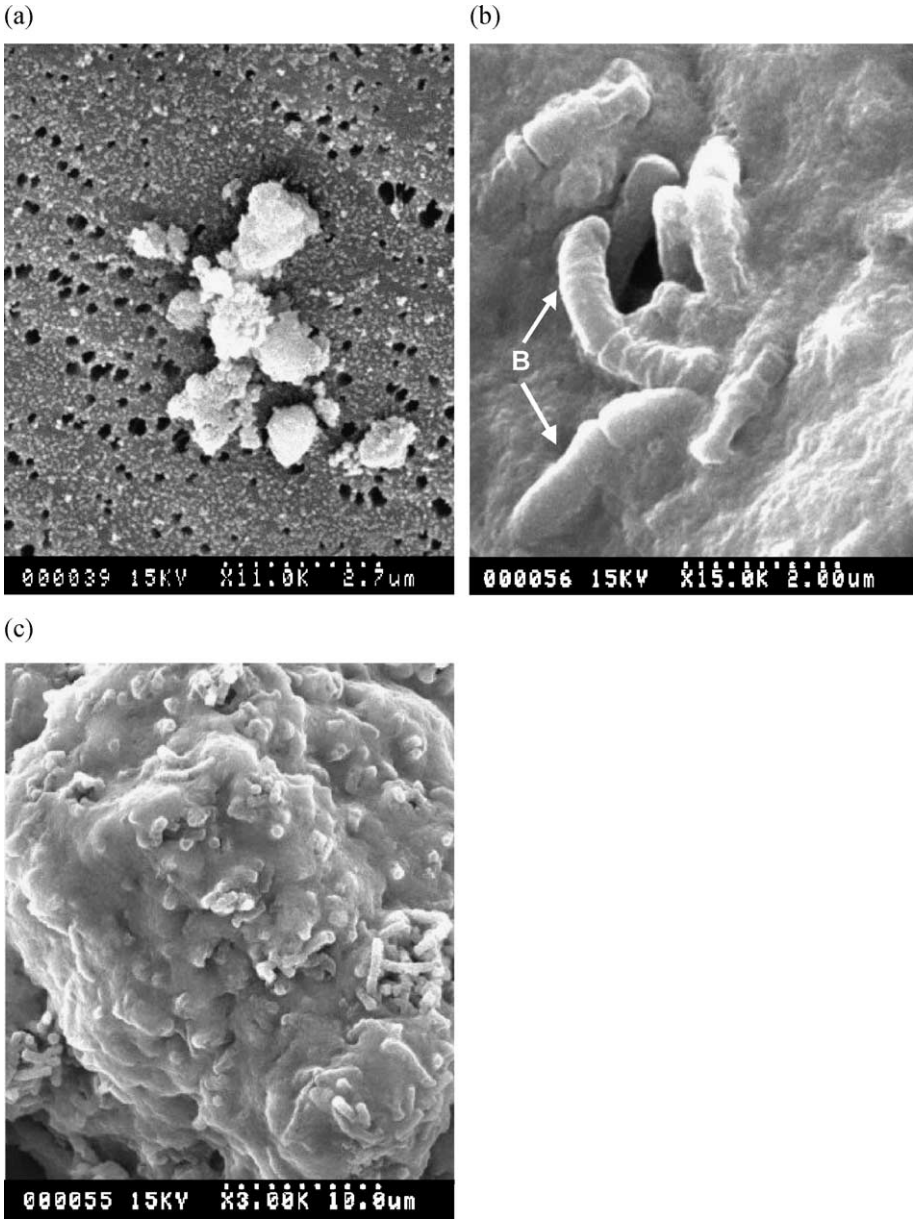


Fig. 2. SEM images of the synthetic ferrihydrite composites after 2 days of heating. Image (a) is ferrihydrite without bacteria, (b) is the bacterial (B) ferrihydrite composite A5 and (c) is a lower magnification image illustrating the distribution of bacterial cells throughout the ferrihydrite matrix.

the binding of ferric iron and nucleation of ferrihydrite to bacterial surface functional groups (i.e., carboxyl and phosphoryl groups) (Fortin et al., 1997; Smith and Ferris, 2003) would have constrained the rotation of the nanoparticles, thereby inhibiting subsequent aggregation and crystal growth according to the model of Banfield et al. (2000). The lack of transformation in samples A6 and A7 attests to the strength of the constraining ability of bacterial surfaces as the same hydrothermal conditions facilitated the rapid transformation of synthetic ferrihydrite to hematite. The peaks in the XRD traces of samples A1–A5 may

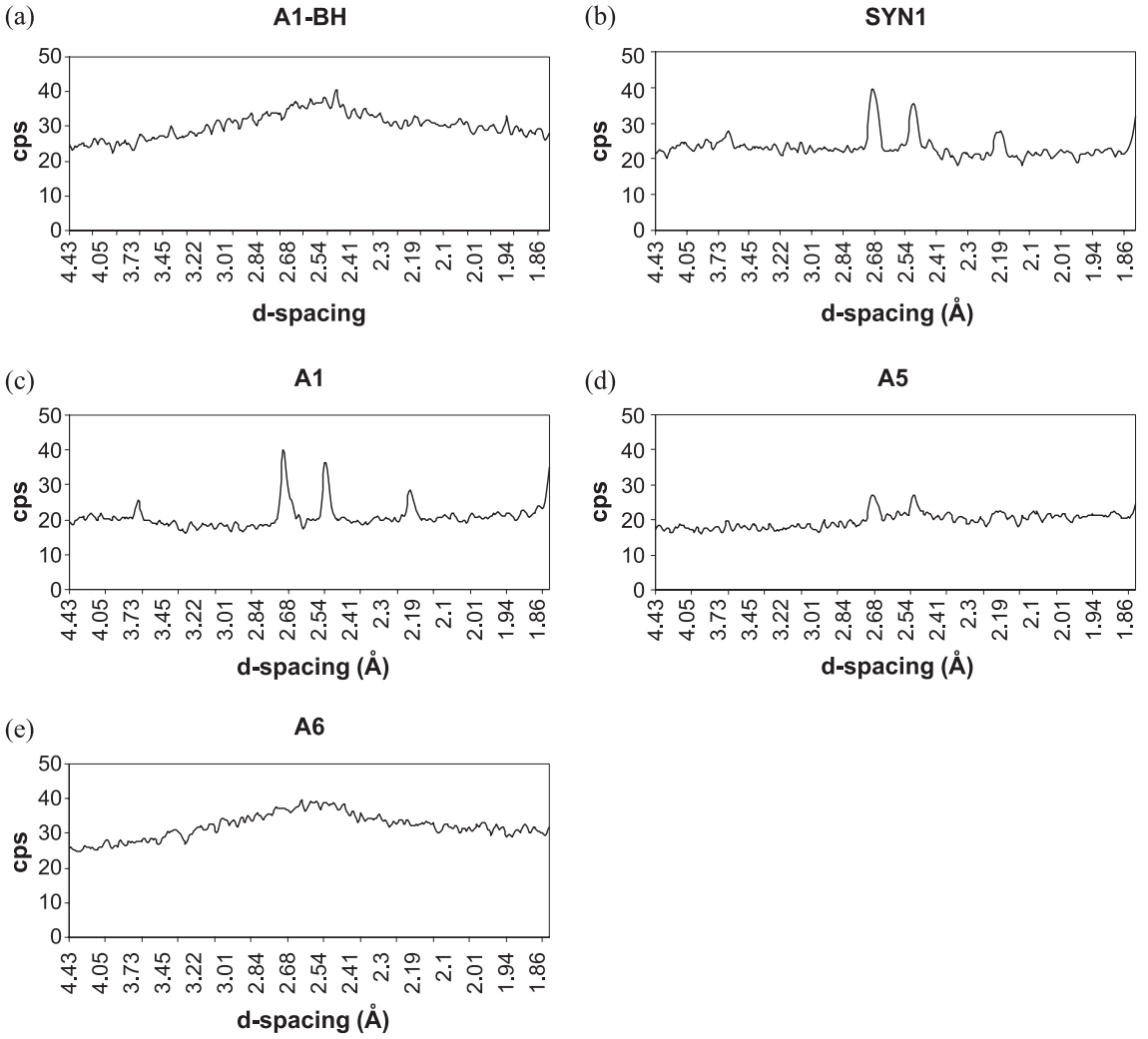


Fig. 3. X-ray diffraction traces of (a) A1 ferrihydrite before heating (BH), (b) synthetic ferrihydrite "SYN1" lacking bacteria after heating and (b, c, d) three other samples after heating illustrating a decrease in peak height in association with increasing amounts of bacteria from A1 through to A6.

be an indication that the increased amount of precipitated ferrihydrite would have created isolated regions in these composites that were not within a close enough proximity to the bacterial surfaces, resulting in some Brownian motion occurring in these regions and minor amounts of hematite forming.

Based on the results of this study, approximately 50% of the total Fe in an aqueous system must be microbially bound as ferric iron, while the remainder exists as nucleated and precipitated ferrihydrite for bacterial-ferrihydrite composites to resist hydrothermal transformation when no other inhibition binding agents such as silica or phosphorus are present (Carlson and Schwertmann, 1981; Barrón et al., 2003). At Axial Volcano, silica and several other elements are present in the seawater and adsorbed to ferrihydrite (Kennedy et al., 2003a,b), which have been shown to inhibit the phase transition of ferrihydrite and likely contribute its stability (Schwertmann and Murad, 1983; Zhao et al., 1994; Kukkadapu et al., 2003). In addition to these abiotic factors, ferrihydrite from Axial Volcano is intermixed

Table 2
Peak heights of the samples from Table 1, reported in counts per second above the background count rate

| Peak (Å) | A1 | A2 | A3 | A4 | A5 | A6 | A7 |
|---|---|---|---|---|---|---|---|
| 3.6 | 4.68 | 8.67 | 1.66 | np | np | np | np |
| 2.7 | 19.51 | 40.94 | 13.76 | 3.85 | 7.24 | np | np |
| 2.5 | 15.13 | 27.67 | 9.91 | 3.14 | 5.29 | np | np |
| 2.2 | 8.12 | 11.24 | 6.51 | np | np | np | np |

np=not present.

with bacteria, which have been shown here to also stabilize ferrihydrite. The mass of bacteria is not capable of being calculated in the sample from Axial Volcano; however, the SEM/TEM image from Fig. 1 illustrates that most of the ferrihydrite exits in contact with a microbial surface. Furthermore, unlike the passive binding of ferrihydrite to *B. subtilus*, iron oxidizing bacteria such as *G. ferruginea*, *L. ochracea* and PV-1 employ specific binding strategies (i.e. stalk, sheath and filament formation) to remove ferrihydrite precipitates from their local environment once Fe(II) has been oxidized (Hallbeck and Pedersen, 1991; Emerson, 2000). This binding pathway, in addition to the visual inspection in Fig. 1, likely results in an increased percentage of ferrihydrite in association with bacteria when compared to the bacterial-synthetic ferrihydrite composites. Consequently, the effect of bacteria should be considered in addition to abiotic factors when predicting and understanding the phase transition pathway of natural bacteriogenic ferrihydrite.

The surface area and density of surface functional groups decreases as ferrihydrite becomes more structurally ordered (Cornell and Schwertmann, 1996; Kennedy et al., 2003b). With the exception of the few elements (i.e. Mn(II) and Ni(II)) that are incorporated into the structure of hematite or goethite, the phase transition of ferrihydrite will generally result in element desorption (Ford et al., 1997). Subsequently, stabilization of the large (250–600 $m^2/g$) and reactive surface area (Dzombak and Morel, 1990; Kennedy et al., 2003b) of ferrihydrite could impart a degree of control on oceanic metal cycling, especially when the strong metal immobilization capacity of these iron oxides (Kennedy et al., 2003b) and the potential extent of these types of deposits (~50,000 km along MORs and perhaps on hundreds of seamounts) (Scott, 1997) is taken into consideration. Moreover, Bau et al. (1996) demonstrated that sorption processes onto hydrous Fe–Mn oxides may be a mechanism for rare earth element anomalies in seawater, making it reasonable to suggest that marine iron oxide deposits also mediate the cycling of other metals. In addition, environmental remediation technologies may be able to utilize the ability of bacteria to stabilize poorly ordered and reactive ferrihydrite so as to ensure prolonged removal of heavy metals from polluted waters (Cornell and Schwertmann, 1996).

The binding of metals on a bacterial surface has been shown to inhibit cell lysis (Ferris et al., 1998), and therefore the binding of ferric iron and precipitation of ferrihydrite on bacteria likely contributes to the preservation and fossilization of iron oxidizing bacteria. Ferrihydrite transformation will ultimately affect bacteria encrusted with ferrihydrite by destroying any morphological evidence of the bacterium's existence. Consequently, the ability of bacteria to inhibit the transformation of ferrihydrite will also promote cellular preservation. To date, there have been numerous suggestions of bacterial microfossils in ancient sediments (Juniper and Fouquet, 1988; Konhauser, 2000; Emerson, 2000), and evidence of these types of microfossils may come from the identification of filamentous bacterial-like forms within material examined in recent studies of low temperature mineral assemblages from museum collections (Hoffmann and Farmer, 2000). Knowing how

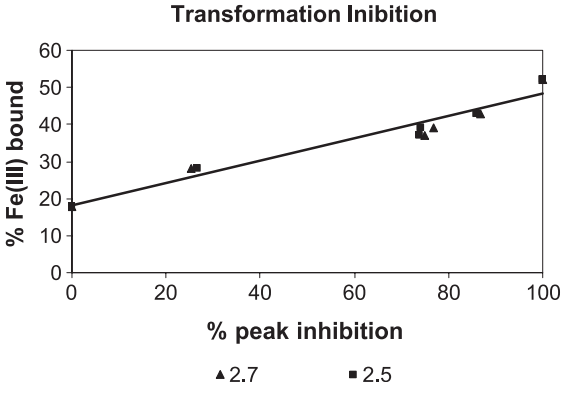


Fig. 4. The percent of ferric iron microbially bound as a function of the percent of ferrihydrite transformation inhibition for both the 2.7 and 2.5 Å XRD trace peaks (denoted 2.7 and 2.5, respectively). The data was curve fitted and the value of complete phase transition inhibition was determined by extrapolation of the *y*-intercept.

to recognize microfossils of iron oxidizing bacteria on Earth would be useful for detecting similar fossilized organisms on Mars or even on Jupiter's moon Europa, where proposed present day geologic activity may be creating hydrothermal vents and exomicrobiological iron oxides.

## Acknowledgements

This work was supported by a Natural Sciences and Engineering Research Council of Canada-Collaborative Research Opportunities grant. We thank Susan Glasauer and an anonymous reviewer for their helpful comments with this manuscript. We also thank all the NeMO scientists and crew aboard the NOAA ship Ronald H. Brown in June 2000 and July 2001. **[LW]**

## References

Alt, J.C., 1988. Hydrothermal oxide and nontronite deposits on seamounts in the eastern pacific. Mar. Geol. 81, 227–239.

Banfield, J.F., Welch, S.A., Zhang, H., Ebert, T.T., Penn, R.L., 2000. Aggregation-based crystal growth and microstructure development in natural iron oxyhydroxide biomineralization products. Science 289, 751–754.

Barrón, V., Torrent, J., Grave, E., 2003. Hydromaghemite, an intermediate in the hydrothermal transformation of 2-line ferrihydrite into hematite. Am. Mineral. 88, 1679–1688.

Bau, M., Koschinsky, A., Dulski, P., Hein, J.R., 1996. Comparison of the partitioning behaviours of yttrium, rare earth elements, and titanium between hydrogenetic marine ferromanganese crusts and seawater. Geochim. Cosmochim. Acta 60, 1709–1725.

Binns, R.A., Scott, S.D., Bogdanov, Y.A., Lisitzin, A.P., Gordeev, V.V., Gurvich, E.G., Finlayson, E.J., Boyd, T., Dotter, L.E., Wheller, G.E., Muravyev, K.G., 1993. Hydrothermal oxide and gold-rich sulfate deposits of Franklin Seamount, Western Woodlark Basin, Papua New Guinea. Econ. Geol. 88, 2122–2153.

Boyd, T., Scott, S.D., Hekinian, R., 1993. Trace element patterns in Fe–Si–Mn oxyhydroxides at three hydrothermally active seafloor regions. Resour. Geol. 17, 83–95.

Carlson, L., Schwertmann, U., 1981. Natural ferrihydrites in surface deposits from Finland and their association with silica. Geochim. Cosmochim. Acta 45, 421–429.

Cornell, R.M., Schwertmann, U., 1996. The Iron Oxides: Structure, Properties, Reactions, Occurrence and Uses. VCH, Germany.

Dzombak, D.A., Morel, F.M.M., 1990. Surface Complexation Modelling: Hydrous Ferric Oxide. John Wiley, New York.

Emerson, D., 2000. Microbial oxidation of Fe(II) and Mn(II) at circumneutral pH. In: Lovely, D.R. (Ed.), Environmental Microbe–Metal Interactions. ASM press, Washington, DC, pp. 31–52.

Emerson, D., Moyer, C.L., 2002. Neutrophilic Fe-oxidizing bacteria are abundant at the Loihi Seamount hydrothermal vents and play a major role in Fe oxide deposition. Appl. Environ. Microbiol. 68, 3085–3093.

Emerson, D., Revsbech, N.P., 1994. Investigation of an iron-oxidizing microbial mat community located near Aarhus, Denmark: field studies. Appl. Environ. Microbiol. 60, 4022–4031.

Ferris, F.G., Fyfe, W.S., Beveridge, T.J., 1998. Metallic ion binding by *Bacillus subtilis*: implications for the fossilization of microorganisms. Geology 16, 149–152.

Ford, R.G., Bertsch, P.M., Farley, K.J., 1997. Changes in transition and heavy metal partitioning during hydrous iron oxide aging. Environ. Sci. Technol. 31, 2028–2033.

Fortin, D., Ferris, F.G., Beveridge, T.J., 1997. Surface-mediated mineral development by bacteria. In: Banfield, J.H., Nealson, K.H. (Eds.), Geomicrobiology: interactions between microbes and minerals, Reviews in Mineralogy vol. 35. The Mineralogical Society of America, pp. 161–177.

Fortin, D., Ferris, F.G., Scott, S.D., 1998. Formation of iron-silicates and iron oxides on bacterial surfaces in samples collected near hydrothermal vents on the Southern Explorer Ridge in the northeast Pacific Ocean. Am. Mineral. 83, 1399–1408.

Hallbeck, L., Pedersen, K., 1991. Autotrophic and mixotrophic growth of *Gallionella ferruginea*. J. Gen. Microbiol. 138, 2657–2661.

Hoffmann, B.A., Farmer, J.D., 2000. Filamentous fabrics in low-temperature mineral assemblages: are they fossil biomarkers? Implications for the search for a subsurface fossil record on the early Earth and Mars. Planet. Space Sci. 48, 1077–1086.

Johnson, H.P., Embley, R.W., 1990. Axial seamount: an active ridge axis volcano on the central Juan de Fuca ridge. J. Geophys. Res., B 95, 12,689–12,696.

Juniper, S.K., Fouquet, Y., 1988. Filamentous iron–silica deposits from modern and ancient hydrothermal sites. Can. Mineral. 26, 859–869.

Juniper, S.K., Sarrazin, J., 1995. Interaction of vent biota and hydrothermal deposits: present evidence and future experimentation. In: Humphris, S.E., Zierenberg, R.A., Mullineaux, L.S., Thompson, R.E. (Eds.), Seafloor Hydrothermal Systems: Physical, Chemical, Biological, and Geological Interactions, Geophysical Monograph vol. 91. American Geophysical Union, pp. 178–193.

Juniper, S.K., Tebo, B.M., 1995. Microbe–metal interactions and mineral deposition at deep-sea hydrothermal vents. In: Karl, D.M. (Ed.), The Microbiology of Deep-Sea Hydrothermal Vents. CRC Press, Boca Raton, pp. 219–253.

Kennedy, C.B., Scott, S.D., Ferris, F.G., 2003. Characterization of bacteriogenic iron oxide deposits from Axial Volcano, Juan de Fuca Ridge, north-east Pacific Ocean. Geomicrobiol. J. 20, 199–214.

Kennedy, C.B., Martinez, R.E., Scott, S.D., Ferris, F.G., 2003. Surface chemistry and reactivity of bacteriogenic iron oxides from Axial Volcano, Juan de Fuca Ridge, north-east Pacific Ocean. Geobiology 1, 59–69.

Konhauser, K.O., 2000. Hydrothermal bacterial biomineralization: potential modern-day analogues for banded iron-formations. In: Glenn, C.R., Perot-Lucas, L., Lucas, J. (Eds.), Marine Authigenesis: From Global to Microbial, Special Publications vol. 66. SEPM, Tulsa, OK, pp. 133–145.

Kukkadapu, R.K., Zachara, J.M., Fredrickson, J.K., Smith, S.C., Dohnalkova, A.C., Russell, C.K., 2003. Transformation of 2-line ferrihydrite to 6-line ferrihydrite under oxic and anoxic conditions. Am. Mineral. 88, 1903–1914.

Penn, R.L., Banfield, J.F., 1999. Morphology development and crystal growth in nanocrystalline aggregates under hydrothermal conditions: insights from titania. Geochim. Cosmochim. Acta 63, 1549–1557.

Schwertmann, U., Murad, E., 1983. Effect of pH on the formation of goethite and hematite from ferrihydrite. Clays Clay Miner. 4, 277–284.

Scott, S.D., 1997. Submarine hydrothermal systems and deposits. In: Barnes, H.L. (Ed.), Geochemistry of Hydrothermal Ore Deposits, (3rd edition). Wiley, New York, pp. 797–869.

Smith, D.S., Ferris, F.G., 2003. Specific surface chemical interactions between hydrous ferris oxide and iron-reducing bacteria determined using p$K_a$ spectra. J. Colloid Interface Sci. 266, 60–67.

Warren, L.A., Ferris, F.G., 1998. Continuum between sorption and precipitation of Fe(III) on microbial surfaces. Environ. Sci. Technol. 32, 2331–2337.

Zhao, J.M., Huggings, F.E., Feng, Z., Huffman, G.P., 1994. Ferrihydrite surface structure and its effects on phase transformation. Clays Clay Miner. 42, 737–746.